LETTER

doi:10.1038/nature12083

Digital cameras with designs inspired by the arthropod eye

Young Min Song[1]*, Yizhu Xie[1]*, Viktor Malyarchuk[1]*, Jianliang Xiao[2]*, Inhwa Jung[3], Ki-Joong Choi[4], Zhuangjian Liu[5], Hyunsung Park[6], Chaofeng Lu[7,8], Rak-Hwan Kim[1], Rui Li[8,9], Kenneth B. Crozier[6], Yonggang Huang[8] & John A. Rogers[1,4]

In arthropods, evolution has created a remarkably sophisticated class of imaging systems, with a wide-angle field of view, low aberrations, high acuity to motion and an infinite depth of field[1–3]. A challenge in building digital cameras with the hemispherical, compound apposition layouts of arthropod eyes is that essential design requirements cannot be met with existing planar sensor technologies or conventional optics. Here we present materials, mechanics and integration schemes that afford scalable pathways to working, arthropod-inspired cameras with nearly full hemispherical shapes (about 160 degrees). Their surfaces are densely populated by imaging elements (artificial ommatidia), which are comparable in number (180) to those of the eyes of fire ants (*Solenopsis fugax*) and bark beetles[4,5] (*Hylastes nigrinus*). The devices combine elastomeric compound optical elements with deformable arrays of thin silicon photodetectors into integrated sheets that can be elastically transformed from the planar geometries in which they are fabricated to hemispherical shapes for integration into apposition cameras. Our imaging results and quantitative ray-tracing-based simulations illustrate key features of operation. These general strategies seem to be applicable to other compound eye devices, such as those inspired by moths and lacewings[6,7] (refracting superposition eyes), lobster and shrimp[8] (reflecting superposition eyes), and houseflies[9] (neural superposition eyes).

Improved understanding of light-sensing organs in biology[1,10–12] creates opportunities for the development of cameras that adopt similar engineering principles, to provide operational characteristics beyond those available with existing technologies[13–19]. The compound eyes of arthropods are particularly notable for their exceptionally wide fields of view, high sensitivity to motion and infinite depth of field[1–3]. Analogous man-made cameras with these characteristics have been of long-standing interest, owing to their potential for use in surveillance devices, tools for endoscopy and other demanding applications. Previous work demonstrates devices that incorporate compound lens systems, but only in planar geometries or in large-scale, handmade curved replicas[20–24]. Constraints intrinsic to such approaches prevent the realization of cameras with the key features present in arthropod eyes: full hemispherical shapes in compact, monolithic forms, with scalability in size, number and configuration of the light-sensing elements (ommatidia).

Here we present a complete set of materials, design layouts and integration schemes for digital cameras that mimic hemispherical apposition compound eyes found in biology. Certain of the concepts extend recent advances in stretchable electronics[25] and hemispherical photodetector arrays[13–18], in overall strategies that provide previously unachievable options in design. Systematic experimental and theoretical studies of the mechanical and optical properties of working devices reveal the essential aspects of fabrication and operation.

Figure 1a presents schematic illustrations of the two main subsystems and methods for their assembly into working hemispherical apposition cameras. The first subsystem provides optical imaging function and defines the overall mechanics; it is a moulded piece of the elastomer poly(dimethylsiloxane) (PDMS, with index of refraction $n \approx 1.43$) that consists of an array of 16×16 convex microlenses (with radius of curvature of each microlens $r \approx 400\ \mu m$) over a square area of $14.72\ mm \times 14.72\ mm$, as shown in Supplementary Fig. 1. Of the 256 microlenses, 180 form working components of the camera, each on a matching cylindrical supporting post (of height $h \approx 400\ \mu m$) connected to a base membrane (of thickness $t \approx 550\ \mu m$).

The second subsystem enables photodetection and electrical readout; it consists of a matching array of thin, silicon photodiodes (active areas $d^2 \approx 160\ \mu m \times 160\ \mu m$) and blocking diodes in an open mesh configuration with capability for matrix addressing. Narrow filamentary serpentine traces of metal (Cr/Au) encapsulated by polyimide serve as electrical and mechanical interconnects. Aligned bonding of these two subsystems places each photodiode at the focal position of a corresponding microlens (Fig. 1b), to yield an integrated imaging system. A key feature enabled by the constituent materials and layouts is a fully isotropic elastic mechanical response to large strain deformation, in any direction. In consequence, hydraulic actuation can deterministically transform the planar layout in which these separate subsystems are constructed and bonded together, into a full hemispherical shape (Fig. 1c), with precise engineering control (radius of curvature of the hemisphere $R \approx 6.96\ mm$) and without any change in optical alignment or adverse effect on electrical or optical performance (see Supplementary Figs 2 and 3 for details).

A complete apposition camera (Fig. 1d) consists of this type of imager, combined with a top perforated sheet and a bottom bulk support, both made of black silicone to eliminate stray light, bonded to the outer and inner surfaces, respectively (Fig. 1e and Supplementary Fig. 8). A thin film insert with metallized contact pads connects to a printed circuit board as an interface to external control electronics.

By analogy to imaging organs in arthropods[12], each microlens and supporting post corresponds to a corneal lens and crystalline cone, respectively; each photodiode is a rhabdom; the black elastomer serves as the screening pigment. A collected set of each of these elements represents an ommatidium.

The dimensions and the mechanical properties of the imaging system are critically important for proper operation. The acceptance angle ($\Delta\varphi$) and the inter-ommatidial angle ($\Delta\Phi$) define the nature of image formation[1,26] (Fig. 1a and Supplementary Fig. 4). Each microlens focuses light incident on it within a cone defined by $\Delta\varphi$. An individual ommatidium samples an angular object space determined by $\Delta\Phi$. For the layouts of Fig. 1a, optical simulation suggests a total field of view of

[1]Department of Materials Science and Engineering, Beckman Institute for Advanced Science and Technology, and Frederick Seitz Materials Research Laboratory, University of Illinois at Urbana-Champaign, Urbana, Illinois 61801, USA. [2]Department of Mechanical Engineering, University of Colorado at Boulder, Boulder, Colorado 80309, USA. [3]Department of Mechanical Engineering, Kyung Hee University, Yongin-si, Gyeonggi-do 446-701, South Korea. [4]Department of Chemistry, University of Illinois at Urbana-Champaign, Urbana, Illinois 61801, USA. [5]Institute of High Performance Computing, A*star, 1 Fusionopolis Way, #16-16 Connexis 138632, Singapore. [6]School of Engineering and Applied Sciences, Harvard University, Cambridge, Massachusetts 02138, USA. [7]Department of Civil Engineering and Soft Matter Research Center, Zhejiang University, Hangzhou 310058, China. [8]Department of Mechanical Engineering, Department of Civil and Environmental Engineering, Northwestern University, Evanston, Illinois 60208, USA. [9]State Key Laboratory of Structural Analysis for Industrial Equipment, Department of Engineering Mechanics, Dalian University of Technology, Dalian 116024, China.
*These authors contributed equally to this work.

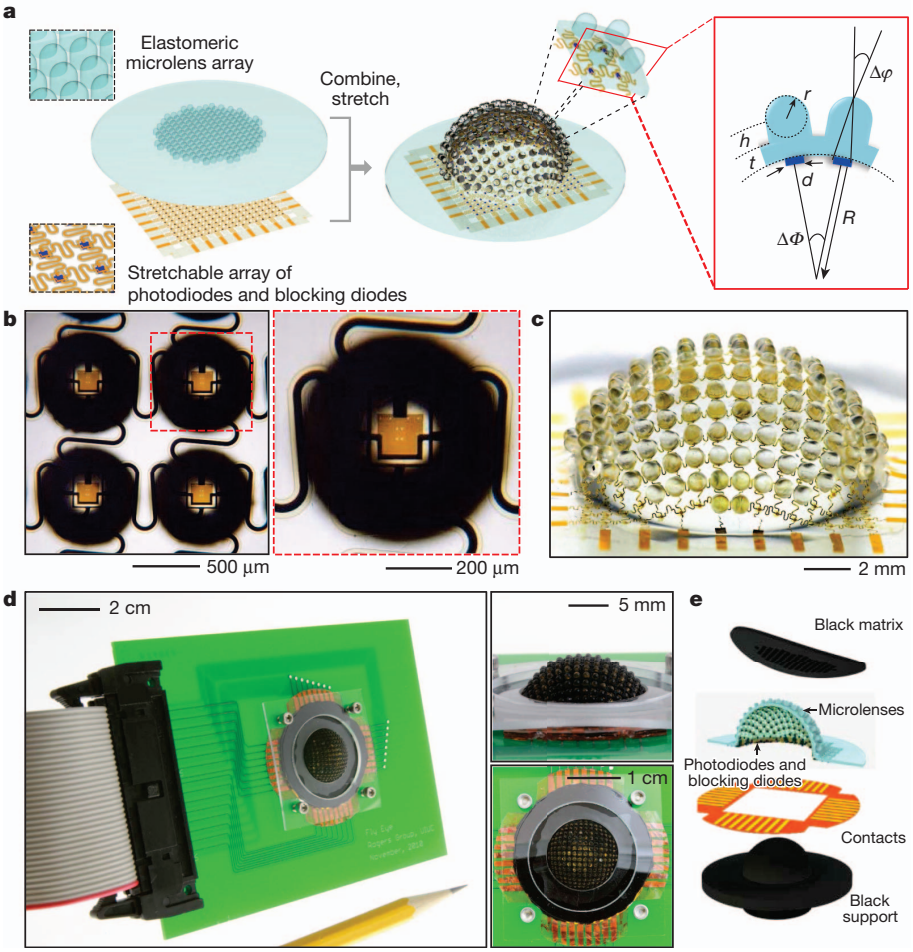

Figure 1 | Schematic illustrations and images of components and integration schemes for a digital camera that takes the form of a hemispherical, apposition compound eye. **a**, Illustrations of an array of elastomeric microlenses and supporting posts joined by a base membrane (above) and a corresponding collection of silicon photodiodes and blocking diodes interconnected by filamentary serpentine wires and configured for matrix addressing (below). On the left, these components are shown in their as-fabricated, planar geometries; the upper and lower insets provide magnified views of four adjacent unit cells (that is, artificial ommatidia). Bonding these two elements and elastically deforming them ('combine, stretch') into a hemispherical shape creates the digital imaging component of an apposition compound eye camera (centre). An exploded view of four adjacent unit cells appears in the centre inset, with a cross-sectional illustration (on the right) that highlights key parameters: the acceptance angle ($\Delta\varphi$) for each ommatidium, the inter-ommatidial angle ($\Delta\Phi$), the radius of curvature of the entire device (R) and of an individual microlens (r), the height of a cylindrical supporting post (h), the thickness of the base membrane (t), and the diameter of the active area of a photodiode (d). **b**, Optical micrograph of four adjacent ommatidia in planar format (left), with magnified view (right). **c**, Image of a representative system after hemispherical deformation. **d**, Photograph of a completed camera mounted on a printed circuit board as an interface to external control electronics (left), with close-ups in the insets (upper inset shows tilted view; lower inset shows top view). **e**, Exploded-view illustration of the components of this system: perforated sheet of black silicone (black matrix), hemispherical array of microlenses and photodiodes/blocking diodes, thin-film contacts for external interconnects, and hemispherical supporting substrate of black silicone.

about 160° when $\Delta\varphi = 9.7°$ and $\Delta\Phi = 11.0°$, without overlapping fields in adjacent ommatidia (that is, $\Delta\varphi < \Delta\Phi$; see Supplementary Figs 5 and 6 for details). The key dimensions of the optical subsystem—d, r and h—provide these features when implemented with PDMS as the optical material (Supplementary Fig. 7). The combined heights of the microlenses, supporting posts and base membrane (that is, $r + h + t$) position the photodiodes at distances of one focal length ($f = rn/(n-1) = r + h + t$) from the lens surface. Collimated light at normal incidence focuses to spot sizes that are smaller (about 100 μm × 100 μm) than the areas of the photodiodes.

Retaining these optical parameters throughout the process of transformation from planar to hemispherical shapes represents a challenge that can be addressed with two new design/integration approaches. The first approach involves a method for bonding the optical and electrical subsystems at the positions of the photodiodes/blocking diodes only. This configuration ensures optical alignment during subsequent deformation, but allows free motion of the serpentine interconnects to minimize their effects on the overall mechanics. The resulting response of the system to applied force is dominated by the elastic behaviour of the PDMS (modulus about 1 MPa), and is nearly independent of the hard materials found in the array of photodiodes/blocking diodes (Si, with modulus about 150 GPa, Au, with modulus about 80 GPa and polyimide, with modulus about 5 GPa)[27,28]. In particular, the computed effective modulus of the system is only 1.9 MPa, with global strains that can reach more than 50% in equi-biaxial tension before exceeding the fracture thresholds of the materials.

The second approach exploits a set of dimensional and material choices in the optical subsystem. Here, the modulus of the PDMS is sufficiently small and the heights of the supporting posts are sufficiently large that deformations induced by stretching the base membrane are almost entirely mechanically decoupled from the microlenses. As a result, large strains created by geometry transformation induce no measurable change in the focusing properties. In addition, the combined heights of the microlenses and the posts are large compared to the thickness of the base membrane. This layout minimizes strain at the locations of bonding with the photodiodes/blocking diodes, thereby eliminating the possibility for failure at these interfaces or in the silicon.

Figure 2 summarizes these features in a series of micro X-ray computed tomography (XCT; MicroXCT 400) images and finite element method (FEM) calculations before and after geometrical transformation (see Supplementary Figs 9 and 10 for additional details of FEM and analytical treatments of the mechanics). The results in Fig. 2c highlight four adjacent ommatidia, with strain distributions determined by FEM in each of the different layers of a single ommatidium. The top and bottom surfaces, where the microlenses and photodiodes are located, respectively, show excellent isolation. The peak strains in these regions are <1% (microlenses in box of Fig. 2c) and <0.2% (photodiode/blocking diodes in box of Fig. 2c) even for the large global strains (about 30% or more) that occur in the hemispherical shape. Quantitative analysis of the distribution of r across the entire array, before and after deformation (top panels of Fig. 2d; Supplementary Fig. 12) shows no change, which is consistent with FEM findings (Supplementary Fig. 13). Non-uniform strains lead to a slight, but systematic, spatial variation of $\Delta\Phi$ across the array (bottom left panel of Fig. 2d), as expected based on the mechanics (Supplementary Fig. 13). All ommatidia have an orientation along the direction of the surface normal (that is, the tilt from normal, θ_{tilt}, is zero; bottom right panel of Fig. 2d).

Working apposition cameras formed in this manner have excellent operational characteristics and high yields. Overall image construction follows from a pointwise sampling by the photodiode/blocking diodes of images formed at each microlens. In this way, each ommatidium contributes a single pixel to a different region of the resultant image. Figure 3a schematically illustrates this process through images computed using physically correct ray-tracing procedures (GNU Goptical, see Supplementary Figs 14 and 15 for details) executed in a parallel fashion. Each microlens produces a small image of an object (in this example, a '+' line-art pattern) with a form dictated by the parameters of the lens and the viewing angle (third panel from the left in Fig. 3a). An individual photodiode generates photocurrent only if a portion of the image formed by the associated microlens overlaps the active area. The photodiodes stimulated in this way produce a sampled image (second panel from the left in Fig. 3a) of the object. In biology, rapid motion of the eye and/or the object can yield improvements in effective resolution. Experiments and modelling reported here simulate such effects by scanning the camera from -5.5° to 5.5° in the θ and φ directions with steps of 1.1°. Modelling results appear in the left panel of Fig. 3a (scans from -11° to 11° lead to complete overlap of contributions from neighbouring ommatidia, thereby allowing subtraction of effects of isolated non-functional elements). Figure 3b presents pictures, rendered on hemispherical surfaces with sizes that match the camera, of two different line-art patterns collected using a representative device, for which 166 out of a total of 180 ommatidia function properly (see Supplementary Fig. 16).

Software algorithms and data acquisition systems enable the cameras to adapt to different light levels. When we use a scanning mode for data collection (see Supplementary Information), the results are remarkably consistent with optical modelling that assumes ideal characteristics for the cameras (Fig. 3c). Systematic, quantitative comparisons between parametric simulations and experimentally recorded images indicate correlation values (91.3% and 89.0% in left and right images, respectively) in a range consistent with operation close to limits dictated by the optics and physical designs. Some loss of resolution and edge definition follows from parasitic scattering within the camera. See Supplementary Figs 18 and 19 for details. Other examples appear in Supplementary Fig. 20.

The arthropod eye offers resolution determined by the numbers of ommatidia, and is typically modest (Fig. 3b and c) compared, for example, to mammalian eyes. Two other attributes, however, provide powerful modes of perception. First, the hemispherical apposition design enables exceptionally wide-angle fields of view, without off-axis aberrations. Figure 4a gives an example of this characteristic, through pictures of a line-art soccer ball illustration placed at three different angular positions: -50° (left), 0° (centre), and 50° (right). All three cases show comparable clarity, without anomalous blurring or aberrations, consistent with the proper, independent functioning of ommatidia across the array. Equivalent imaging modes are difficult or impossible to obtain using planar detector technologies even with sophisticated fish-eye lenses, spherical mirrors or other specialized optics. Quantitative analysis can be performed through laser illumination at angles ranging from -80° to 80° with 20° steps along both the x and y directions, as shown in a single composite image in Fig. 4b (see individual images in Supplementary Fig. 21). The uniformity in sizes, shapes, illumination levels and positions of these spots are consistent with expected behaviour over the entire approximately 160° field of view.

The second attribute is the nearly infinite depth of field that results from the short focal length of each microlens and the nature of image formation[3]. In particular, as an object moves away from the camera, the size of the image decreases but remains in focus (Supplementary Fig. 22). A consequence is that the camera can accurately and

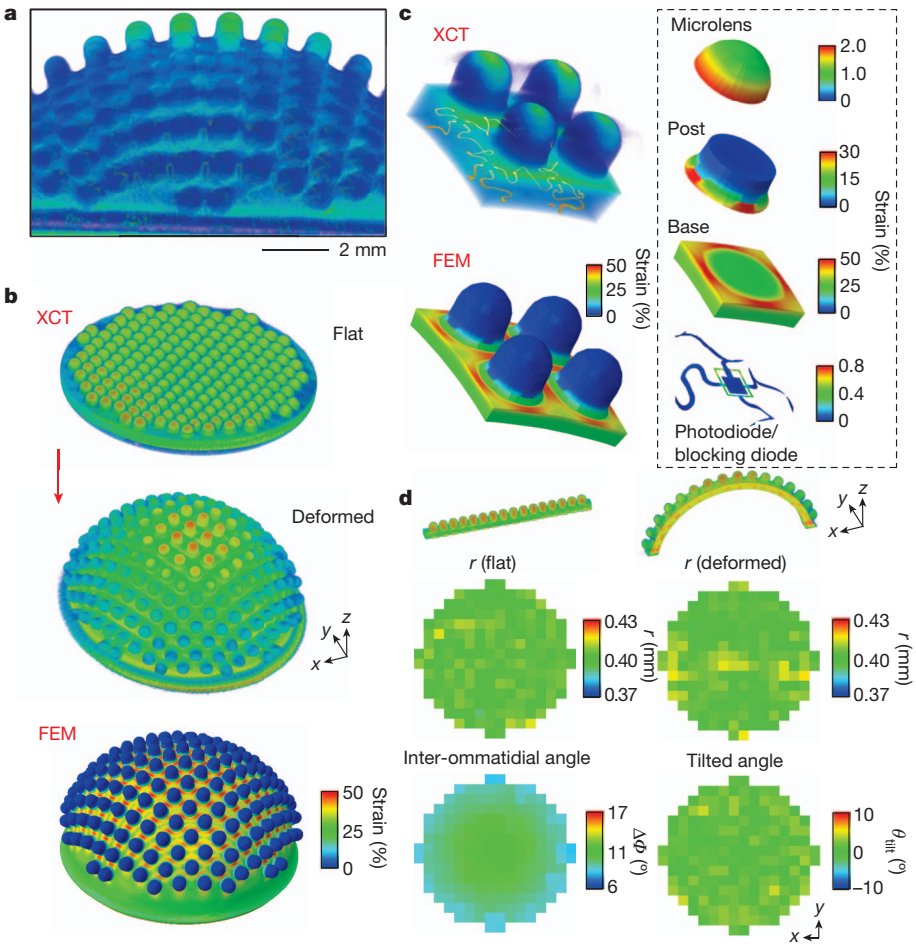

Figure 2 | Computational and experimental studies of the mechanics associated with assembly of a hemispherical, apposition compound eye camera. **a**, XCT image of the imaging component of the camera, showing both the microlenses and the photodiodes/blocking diodes with serpentine interconnects (see Supplementary Fig. 11 for additional details of XCT). **b**, XCT images before (top) and after (middle) elastic deformation into a hemispherical shape, and FEM results for the system after deformation (bottom). **c**, High-resolution XCT image of four adjacent ommatidia located slightly off-axis (in polar and azimuth angles) near the centre of a camera, and FEM computed shape and distributions of strain at this location. The boxed panels highlight strains in different regions of a single ommatidium: microlens, cylindrical post, membrane base and photodiode/blocking diode island with serpentine interconnects. **d**, The top panels are XCT images of 16 microlenses from the middle row of an array in flat (left) and hemispherical (right) geometries. The middle panels are colour maps of the radii of curvature (r) of microlenses in the array, in flat (left) and hemispherical deformed (right) geometries. The bottom panels are colour maps of $\Delta\Phi$ (left) and the angle of tilt of ommatidia away from the surface normal θ_{tilt} (right); both in the hemispherical deformed configuration.

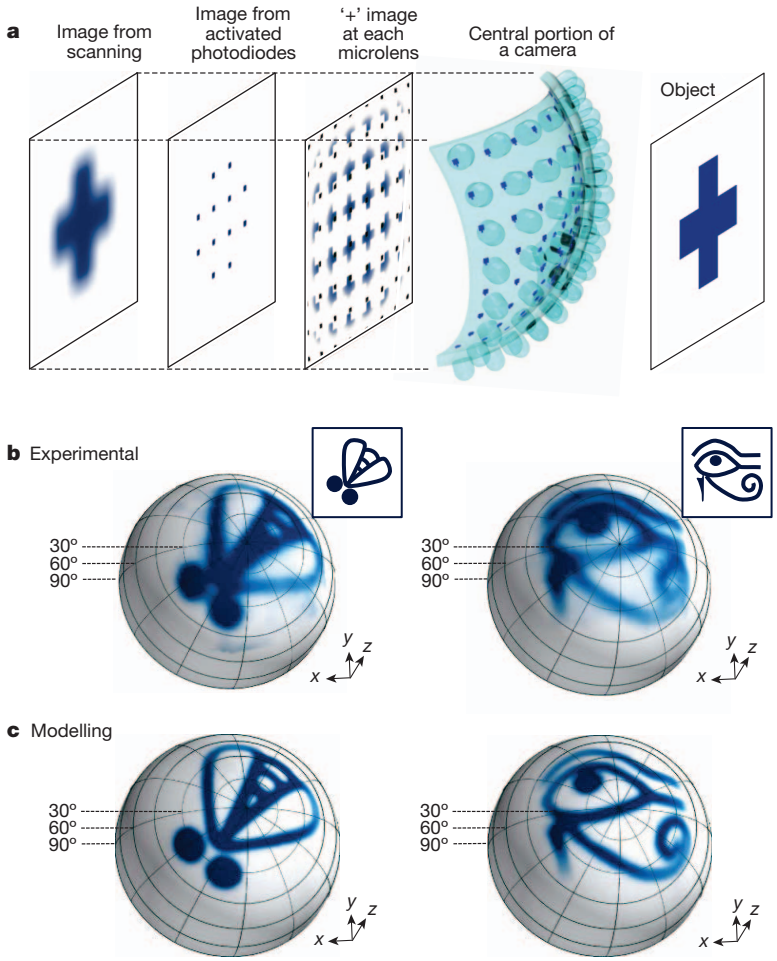

Figure 3 | Operating principles of a hemispherical, apposition compound eye camera and representative pictures. **a**, Conceptual view of image formation, illustrated by quantitative ray-tracing results for the simple case of an 8×8 hemispherical array of ommatidia, corresponding to the central region of the camera. Each microlens generates an image of the object ('+' pattern in this example), with characteristics determined by the viewing angle. Overlap of a portion of each image with the active area of a corresponding photodiode (black squares in the third frame from left) generates a proportional photocurrent at this location of the array (second frame from left). The result is a sampled reproduction of the object. Improved effective resolution can be realized by scanning the camera (from -5.5° to 5.5° in the θ and φ directions with 1.1° steps, as shown in the left frame). **b**, Pictures (main panels) of line-art illustrations of a fly (left inset) and a 'Horus eye' (an Egyptian hieroglyphic character) (right inset) captured with a hemispherical, apposition compound eye camera, each rendered on a hemispherical surface that matches the shape of the device. Experimental setups appear in Supplementary Fig. 17. **c**, Images as in **b**, computed by ray-tracing analysis, assuming ideal construction and operation of the camera.

simultaneously render pictures of multiple objects in a field of view, even at widely different angular positions and distances. Figure 4d presents the results of demonstration experiments. Even though movement of the object away from the camera changes its size in the corresponding image, the focus is maintained. Objects with the same angular size that are located at different distances produce images with the same size, all of which is consistent with modelling (Supplementary Fig. 23).

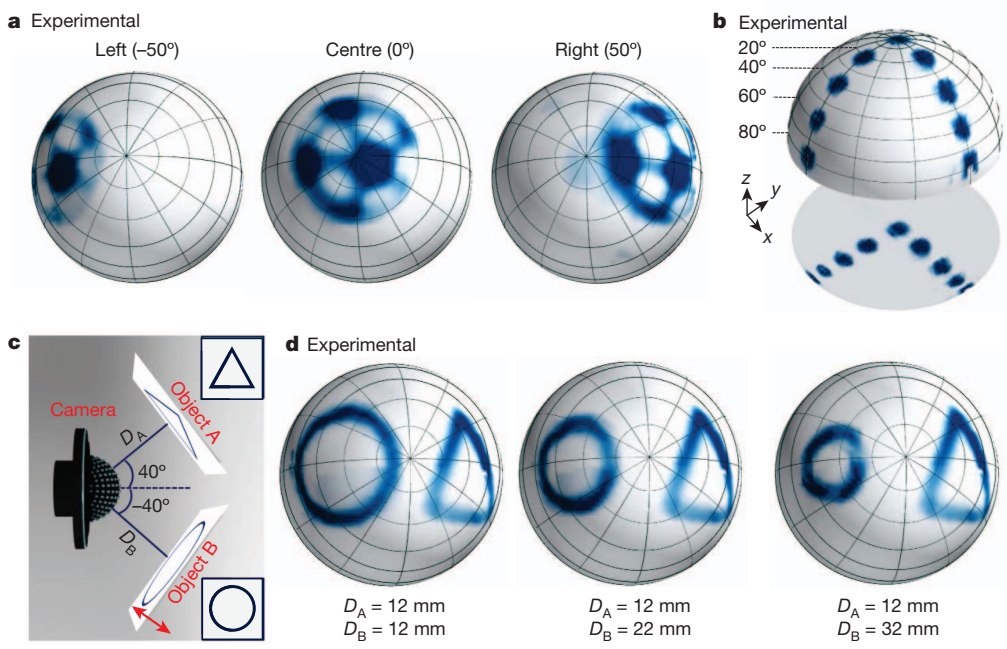

Figure 4 | Imaging characteristics of a hemispherical, apposition compound eye camera. **a**, Pictures of a soccer ball illustration captured at three different polar angles relative to the centre of the camera: -50° (left), 0° (centre), and 50° (right). **b**, Composite picture corresponding to sequential illumination of the camera with a collimated laser beam at a nine different angles of incidence (from -80° to 80° in both x and y directions, with 20° steps), displayed on a hemispherical surface (top) and projected onto a plane (bottom). **c**, Schematic illustration of an experimental setup to demonstrate key imaging characteristics. One object (object A, triangle) lies at an angular position of 40° and distance D_A; the other (object B, circle) at -40° and D_B. **d**, Pictures of these objects collected at different values of D_B.

The cameras reported here incorporate approximately twice as many ommatidia (about 180) as eyes found in some worker ants (about 100 in *Linepithema humile*)[29], significantly fewer than in dragonflies (about 28,000 in *Anax junius*)[10] or praying mantises (about 15,000 in *Stagmatoptera biocellata*)[30], but all with similar fields of view (an estimated 140–180 degrees).

A key defining attribute of our elastomeric optical and deformable electronic subsystems is their applicability to devices with large numbers of ommatidia, diverse spatial layouts, and dimensions into the micrometre regime. Compatibility with silicon technology suggests that commercially available sophistication in imaging arrays and straightforward advances in assembly hardware can enable apposition cameras with resolution and other capabilities that significantly exceed those in known species of arthropods. Specific application requirements and design considerations will dictate the choice between apposition cameras and more conventional approaches that use advanced imaging systems based on fish-eye lenses and others. Other important directions for future research include efforts to expand capabilities beyond those found in biology, such as engineering systems for continuous tuning of the curvature of the hemispherical supporting substrate. Biologically inspired schemes for adapting to different light levels are also of interest.

METHODS SUMMARY

The optical subsystem was formed by casting and curing a prepolymer to PDMS (Sylgard 184, Dow Corning) against a precision, micro-machined aluminium mould and associated fixture. Release of the cured PDMS yielded microlenses and supporting posts with a thin PDMS membrane as a base, each with well defined dimensions. Fabrication of the electrical subsystem involved a series of thin-film processing steps conducted on a silicon-on-insulator wafer. As a final step, etching with concentrated hydrofluoric acid removed the buried oxide layer. Subsequent transfer printing onto the rear plane of the optical subsystem used a homebuilt apparatus, with integrated microscope stage to enable precise alignment. Irreversible bonding at the positions of the photodiodes/blocking diodes was enabled by layers of SiO_2 deposited only in these regions, to allow condensation reactions between their hydroxyl-terminated surfaces and those of the PDMS. A polyimide film with metal contact pads was mounted onto the periphery of the resulting system with an adhesive. A custom mounting assembly and sealed chamber enabled hydraulic deformation from a planar to hemispherical geometry. A hemispherical supporting rod made of PDMS mixed with black silicone pigment (Smooth-on Inc.), and coated with a thin layer of adhesive, held the system in its deformed, hemispherical geometry. A perforated sheet of black silicone, formed by laser machining of thin film membrane (Ecoflex, Smooth-on) mixed with carbon black powder (Strem Chemical), was manually stretched and assembled onto the imager. Mounting on a printed circuit board using mechanical pressure applied with a plastic frame established good electrical contact between the printed circuit board and the metal contacts on the polyimide film. The completed cameras collected pictures of opaque line-art patterns on transparency foils illuminated from behind with diffuse white light, using automated scanning and data acquisition systems.

Received 21 January; accepted 18 March 2013.

1. Warrant, E. & Nillson, D.-E. *Invertebrate Vision* Ch. 1 (Cambridge Univ. Press, 2006).
2. Dudley, R. *The Biomechanics of Insect Flight: Form, Function, Evolution* Ch. 5 (Princeton Univ. Press, 2000).
3. Floreano, D., Zufferey, J.-C., Srinivasan, M. V. & Ellington, C. *Flying Insects and Robot* Ch. 10 (Springer, 2009).
4. Wheeler, W. M. *Ants: their Structure, Development and Behavior* Ch. 4 (Columbia Univ. Press, 1910).
5. Chapman, J. A. Ommatidia numbers and eyes in Scolytid beetles. *Ann. Entomol. Soc. Am.* **65,** 550–553 (1972).
6. Horridge, G. A., McLean, M., Stange, G. & Lillywhite, P. G. A diurnal moth superposition eye with high resolution *Phalaenoides tritifica* (Agaristidae). *Proc. R. Soc. Lond. B* **196,** 233–250 (1977).
7. Kral, K. & Stelzl, M. Daily visual sensitivity pattern in the green lacewing *Chrysoperla carnea* (Neuroptera: Chrysopidae). *Eur. J. Entomol.* **95,** 327–333 (1998).
8. Nilsson, D.-E. A new type of imaging optics in compound eyes. *Nature* **332,** 76–78 (1988).
9. Zeil, J. A new kind of neural superposition eye: the compound eye of male Bibionidae. *Nature* **278,** 249–250 (1979).
10. Land, M. F. & Nillson, D.-E. *Animal Eyes* (Oxford Univ. Press, 2002).
11. Land, M. F. The optics of animal eyes. *Contemp. Phys.* **29,** 435–455 (1988).
12. Nillson, D.-E. Vision optics and evolution. *Bioscience* **39,** 298–307 (1989).
13. Ko, H. C. *et al.* A hemispherical electronic eye camera based on compressible silicon optoelectronics. *Nature* **454,** 748–753 (2008).
14. Jung, I. *et al.* Dynamically tunable hemispherical electronic eye camera system with adjustable zoom capability. *Proc. Natl Acad. Sci. USA* **108,** 1788–1793 (2011).
15. Hung, P. J., Jeong, K., Liu, G. L. & Lee, L. P. Microfabricated suspensions for electrical connections on the tunable elastomer membrane. *Appl. Phys. Lett.* **85,** 6051–6053 (2004).
16. Jeong, K., Kim, J. & Lee, L. P. Biologically inspired artificial compound eyes. *Science* **312,** 557–561 (2006).
17. Dinyari, R., Rim, S.-B., Huang, K., Catrysse, P. B. & Peumans, P. Curving monolithic silicon for nonplanar focal plane array applications. *Appl. Phys. Lett.* **92,** 191114 (2008).
18. Xu, X., Davanco, M., Qi, X. F. & Forrest, S. R. Direct transfer patterning on three dimensionally deformed surfaces at micrometer resolutions and its application to hemispherical focal plane detector arrays. *Org. Electron.* **9,** 1122–1127 (2008).
19. Street, R. A., Wong, W. S. & Lujan, R. Curved electronic pixel arrays using a cut and bend approach. *J. Appl. Phys.* **105,** 104504 (2009).
20. Tanida, J. *et al.* Thin observation module by bound optics (TOMBO): concept and experimental verification. *Appl. Opt.* **40,** 1806–1813 (2001).
21. Duparré, J., Wippermann, F., Dannberg, P. & Reimann, A. Chirped arrays of refractive ellipsoidal microlenses for aberration correction under oblique incidence. *Opt. Express* **13,** 10539–10551 (2005).
22. Li, L. & Yi, A. Y. Development of a 3D artificial compound eye. *Opt. Express* **18,** 18125–18137 (2010).
23. Franceschini, N., Pichon, J. M. & Blanes, C. From insect vision to robot vision. *Phil. Trans. R. Soc. Lond. B* **337,** 283–294 (1992).
24. Afshari, H. *et al.* The PANOPTIC camera: a plenoptic sensor with real-time omnidirectional capability. *J. Sign. Process Syst.* http://dx.doi.org/10.1007/s11265-012-0668-4 (2012).
25. Someya, T. *Stretchable Electronics* (Wiley, 2013).
26. Land, M. F. Visual acuity in insects. *Annu. Rev. Entomol.* **42,** 147–177 (1997).
27. Wang, S. *et al.* Mechanics of curvilinear electronics. *Soft Matter* **6,** 5757–5763 (2010).
28. Lu, C. *et al.* Mechanics of tunable hemispherical electronic eye camera systems that combine rigid device elements with soft elastomers. *J. Appl. Mech.* (in the press).
29. Wild, A. L. *Taxonomic Revision of the Ant Genus* Linepithema *(Hymenoptera: Formicidae)* (Univ. California Press, 2007).
30. Barrós-Pita, J. C. & Maldonado, H. A fovea in the praying mantis eye II. Some morphological characteristics. *Z. Vgl. Physiol.* **67,** 79–92 (1970).

Supplementary Information is available in the online version of the paper.

Acknowledgements The work on integration schemes and mechanical designs was supported by the Defense Advanced Research Projects Agency (DARPA) Nanoelectromechanical /Microelectromechanical Science & Technology (N/MEMS S&T) Fundamentals programme under grant number N66001-10-1-4008 issued by the Space and Naval Warfare Systems Center Pacific (SPAWAR). The work on materials, optical modelling and imaging aspects was supported by the National Science Foundation through an Emerging Frontiers in Research and Innovation (EFRI) programme.

Author Contributions Y.M.S., Y.X., V.M., J.X. and J.A.R. designed the experiments, Y.M.S., Y.X., V.M., J.X., I.J., K.-J.C., Z.L., H.P., C.L., R.-H.K., R.L., K.B.C., Y.H. and J.A.R. performed the experiments and analysis. Y.M.S., V.M., J.X. and J.A.R. wrote the paper.

Author Information Reprints and permissions information is available at www.nature.com/reprints. The authors declare no competing financial interests. Readers are welcome to comment on the online version of the paper. Correspondence and requests for materials should be addressed to J.A.R. (jrogers@illinois.edu).